Acta Crystallographica Section D
Biological Crystallography
ISSN 0907-4449

Structure of *Plasmodium falciparum* dihydroorotate dehydrogenase with a bound inhibitor

Darrell E. Hurt,[a] Joanne Widom[a] and Jon Clardy[b]*

[a]Department of Chemistry and Chemical Biology, Cornell University, Ithaca, NY 14850, USA, and [b]Department of Biological Chemistry and Molecular Pharmacology, Harvard Medical School, Boston, MA 02115, USA

Correspondence e-mail: jon_clardy@hms.harvard.edu

Received 12 September 2005
Accepted 20 December 2005

PDB Reference: *P. falciparum* dihydroorotate dehydrogenase, 1tv5, r1tv5sf.

Membrane-associated dihydroorotate dehydrogenase (DHODH) is an antimalarial therapeutic target without an effective inhibitor. Studies on human DHODH (HsDHODH) led to a structural mechanistic model in which respiratory quinones bind in a tunnel formed by the highly variable N-terminus that leads to the flavin mononucleotide-binding site. The therapeutic agents leflunomide (Arava) and brequinar sodium inhibit HsDHODH by binding in this tunnel. *Plasmodium falciparum* DHODH (PfDHODH) and HsDHODH have markedly different sensitivities to the two drugs. To understand the structural basis of this differential sensitivity and begin a structure-based drug-design cycle for PfDHODH inhibitors, the three-dimensional structure (2.4 Å, R = 20.1%) of PfDHODH bound to the active metabolite of leflunomide was determined by X-ray crystallography. Comparison of the structures of HsDHODH and PfDHODH reveals a completely different binding mode for the same inhibitor in these two catalytically identical enzymes and explains the previously observed species-specific preferential binding. Because no effective inhibitors have been described for PfDHODH, this structure provides critical insight for the design of potential antimalarials.

1. Introduction

Dihydroorotate dehydrogenase (DHODH), which catalyzes the rate-limiting step of *de novo* pyrimidine biosynthesis, oxidizes dihydroorotate to orotate using a flavin prosthetic group that couples dihydroorotate oxidation to respiratory quinone reduction. In subsequent biosynthetic steps, orotate is further modified to produce uridine monophosphate, the precursor to all the other pyrimidines used to synthesize DNA, RNA and various cofactors. Pyrimidines also play key roles in protein glycosylation, membrane lipid biosynthesis and strand-break repair (Löffler *et al.*, 1997). DHODH inhibition forms the basis for drugs developed to treat cancer, transplant rejection, rheumatoid arthritis, psoriasis and autoimmune diseases (Kovarik & Burtin, 2003). Additionally, DHODH inhibitors have been suggested as antibiotics (Marcinkeviciene *et al.*, 2000), especially against *Helicobacter pylori* (Copeland *et al.*, 2000), and as antifungal agents (Gustafson *et al.*, 1996).

Plasmodium falciparum, the major human malarial parasite, is particularly susceptible to DHODH inhibition. No pyrimidine-salvage pathways have been detected in the fully sequenced *P. falciparum* genome, suggesting an absolute requirement for *de novo* pyrimidine biosynthesis at least during the parasite's intraerythrocytic stage (Gardner *et al.*, 2002). Small interfering RNA experiments have experimentally verified the requirement of the intraerythrocytic form of

P. falciparum for DHODH activity (McRobert & McConkey, 2002). Other methods have also shown that *P. falciparum* DHODH (PfDHODH) would be a valid target for small-molecule antimalarial therapeutic agents (Baldwin *et al.*, 2002, 2005).

DHODHs form two families: a cytosolic family found mostly in prokaryotes that uses various soluble molecules as electron sinks and a membrane-associated family found mostly in eukaryotes, including *P. falciparum*, that uses respiratory quinones exclusively as the distal electron receptor (Nagy *et al.*, 1992). Although the two families share little sequence identity, structural studies (Hansen *et al.*, 2004; Liu *et al.*, 2000; Nørager *et al.*, 2002; Rowland *et al.*, 1997) revealed that the families share a large α/β-barrel core domain that contains the flavin prosthetic group and forms the active site for dihydroorotate. In family 1 DHODHs this core domain is the entire protein, but in family 2 DHODHs an additional N-terminal domain provides the membrane association needed to allow the access of respiratory quinones (Björnberg *et al.*, 1997; Hansen *et al.*, 2004; Jensen & Björnberg, 1998).

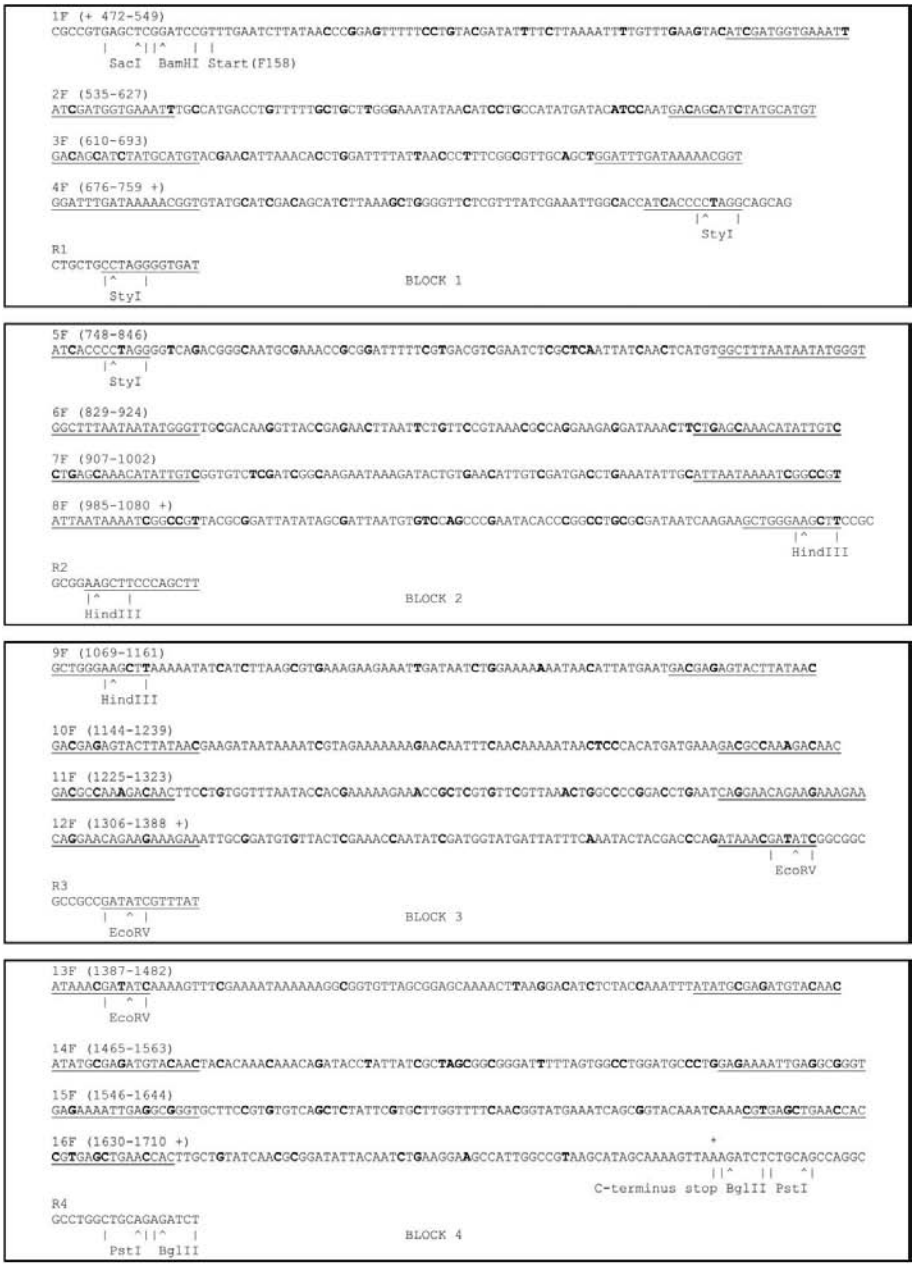

Figure 1
The cDNA sequence for the construct (1.3 kbp) was divided into four blocks of about 300 bases each. Each block was synthesized independently by using four forward primers (1–16F) of about 100 nucleotides each and one reverse primer of about 18 nucleotides (R1–4). Number ranges indicate sequence numbering; + indicates the presence of nucleotides that are not part of the gene. Overlapping residues for primer extension are underlined. Each primer included restriction sites (indicated below the sequence line) for ligating the completed blocks and for future cloning. Silent mutations to introduce restriction sites and *E. coli* codons are indicated in bold.

The N-terminal domain contains two α-helices that are the hallmark of all family 2 DHODHs and which provide a distinct binding site for respiratory quinones. Additionally, in eukaryotic family 2 DHODHs the quinone-binding site is preceded by a putative mitochondrial signaling sequence and a single transmembrane helix (Krogh *et al.*, 2001; Moller *et al.*, 2001; Sonnhammer *et al.*, 1998) which anchors the protein onto the outer surface of the inner mitochondrial membrane. Human DHODH (HsDHODH) retains full *in vitro* (Copeland *et al.*, 1995; Davis *et al.*, 1996), but not *in vivo* (Löffler *et al.*, 2002; Rawls *et al.*, 2000), activity upon truncation of the signal peptide and transmembrane helix. The loss of *in vivo* activity is attributed to improper cellular localization.

Membrane-associated DHODH activity can be abrogated by inhibitors that bind in either the dihydroorotate-binding site or the quinone-binding site. The sequence of the dihydroorotate-binding site is highly conserved, but the sequence of the quinone-binding N-terminal domain is highly variable (Thompson *et al.*, 1994). The variability of the N-terminal domain is thought to be responsible for the high degree of species-related preferential inhibition observed among DHODH family 2 members. For example, the active metabolite of leflunomide (Arava), A77 1726, binds in the tunnel-like quinone-binding site of the N-terminal domain (Liu *et al.*, 2000). A series of A77 1726 analogues inhibit HsDHODH 2000–5700 times more potently than PfDHODH (Baldwin *et al.*, 2002). No potent inhibitors of PfDHODH are known. A crystallographic analysis of

PfDHODH was undertaken to demonstrate the structural differences and species-related inhibitor preferences between HsDHODH and PfDHODH and to begin a cycle of drug design.

2. Materials and methods

2.1. Gene synthesis

Because the A/T-rich sequence and unusual codon usage of *P. falciparum* could lead to difficulties in expressing the parasite's proteins in bacterial expression systems, we synthesized the cDNA from oligonucleotides with *Escherichia coli* codon preferences and the amino-acid sequence for PfDHODH (Fig. 1). The 5′ end of the synthetic cDNA starts at nucleotide 475 (amino acid 159) of the full-length sequence (LeBlanc & Wilson, 1993). This position was chosen based on a multiple sequence alignment (Fig. 2) to correspond to the 5′ end of the N-terminally truncated HsDHODH used in previous structural studies (Liu *et al.*, 2000) that is soluble and fully functional (Copeland *et al.*, 1995). The 3′ end of the construct corresponds to the C-terminus of the protein.

The procedure for the synthesis of the construct by PCR overlap extension was adapted from a published procedure (Horton *et al.*, 1989). Fig. 1 details the synthesis and primers used. The construct was divided into four blocks, each of which would be synthesized by overlap extension. Each PCR reaction was limited to ten cycles using *Pwo* polymerase (Roche) to minimize amplification errors. The product of each reaction was gel purified before serving as a template for the succeeding step. Sequencing ensured no PCR error. Restriction sites were engineered as silent mutations into each block, permitting ligation into the pSTBlue (Novagen) vector for cloning in DH5α (Invitrogen) cells. After cloning, the blocks were excised from the vector, digested by the appropriate restriction enzymes and then ligated together to form the full construct. The synthetic DNA sequence has been deposited in the GenBank database under accession No. AY685129.

2.2. Expression and purification

The PfDHODH DNA construct was introduced into the pRSET expression vector (Invitrogen), which includes an N-terminal polyhistidine (6 × His) tag. PfDHODH was expressed in LB media at 293 K using either freshly transformed or glycerol stocked BL21-CodonPlus(DE3)-RIL (Stratagene) with overnight induction by 10 µ*M* isopropyl β-D-thiogalactoside.

All purification steps were performed at 277 K. Soluble PfDHODH was obtained by sonicating cells resuspended in lysis buffer {1 *M* NaCl, 100 m*M* HEPES pH 8.0, 1 m*M* sodium azide, 0.05%(*w*/*v*) THESIT detergent [$C_{12}E_{\sim 9}$, CMC = 0.005%(*w*/*v*)]} with a non-EDTA-containing protease-inhibitor cocktail (Sigma). After soniciation, the mixture was stirred vigorously for 30 min.

After clarification, the extract was applied onto a pre-equilibrated low-pressure *t*-butyl hydrophobic interaction column and washed in lysis buffer. PfDHODH was readily eluted with a low-salt buffer [100 m*M* NaCl, 50 m*M* HEPES pH 8.0, 1 m*M* sodium azide, 0.05%(*w*/*v*) THESIT] in a single-step gradient. The effluent from the hydrophobic interaction column was immediately applied onto a low-pressure column of pre-equilibrated Talon cobalt-affinity beads (Clontech) and washed with the low-salt buffer. PfDHODH was eluted from the column with a small amount of low-salt buffer supplemented with 100 m*M* imidazole pH 8.0. The effluent from the cobalt-affinity column was concentrated to a volume of 1–2 ml by ultrafiltration and then passed through a HiPrep Sephacryl S-200 HR gel-filtration column pre-equilibrated with crystallization buffer [15 m*M* NaCl, 10 m*M* HEPES pH 7.4, 5 m*M* pentaethylene glycol monooctyl ether (C_8E_5, CMC = 7.1 m*M*)]. The effluent peak corresponding to a protein of about 50 kDa was collected and concentrated by ultrafiltration to a final concentration of about 20 mg ml^{-1}.

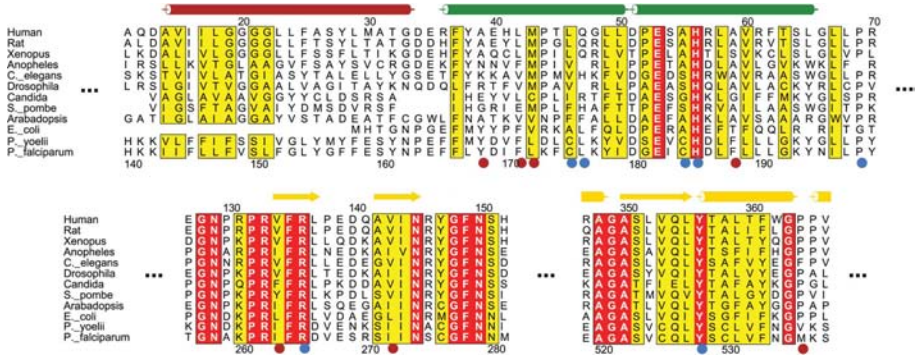

Figure 2
Primary sequence alignment of the binding site. The species for alignment were selected from their importance as laboratory models. The wild-type DHODH sequences were aligned using *CLUSTALW* (Thompson *et al.*, 1994) as implemented on the *MultAlin* server (Corpet, 1988). The sequences shown are an extract of the whole alignment and comprise the quinone-binding site. Secondary structure is indicated for the predicted transmembrane helix (brick), the N-terminal helices that form the site (green) and other parts of the core that complete the site (gold). Numbers above the alignment give the residue number in human and rat DHODH. Numbers below are for PfDHODH. Identical (red) and conserved (yellow) residues are boxed and shaded. The residues most responsible for the overall shape of the quinone-binding tunnel are indicated by dots under the sequence alignment. Red dots mark residues that have significant impact on the shape and chemical environment of the PfDHODH quinone-binding tunnel compared with HsDHODH.

2.3. Enzyme activity

We employed a dye-based assay (Copeland *et al.*, 1995) to determine the kinetic parameters for PfDHODH and to evaluate the inhibitory effect of several compounds, including brequinar, A77 1726, atovaquone (GlaxoSmithKline), DPC-AE661100 ($C_{30}H_{29}N_5O_4$, a proprietary inhibitor of HsDHODH generously donated by Glenn McConkey) and a series of asymmetric terphenyl compounds (Sutton & Clardy, 2001). The decrease

in light absorbance at 595 nm of a protein solution was measured every 30 s over a course of 5 min. This decrease in absorbance corresponds to the reduction of 2,6-dichloroindophenol (DCIP, $\varepsilon = 18.8\ \mathrm{m}M^{-1}\ \mathrm{cm}^{-1}$), which is stoichiometrically coupled to the reduction of quinone substrate. Experiments to determine K_m and k_cat were conducted with six repetitions by varying the concentration of the electron receptor 2,3-dimethoxy-5-methyl-6-(3-methyl-2-butenyl)-1,4-benzoquinone (CoQ_1; 25–100 μM) under conditions of a saturating concentration (250 μM) of dihydroorotate. All experiments were conducted in a solution of 100 mM Tris pH 8.0, 0.1%(w/v) Triton X-100, 68 μM DCIP and 0.004%(w/v) gelatine at room temperature. Inhibition measurements were conducted in triplicate at various concentrations of both inhibitor (15–60 μM) and CoQ_1 (25–100 μM). Reactions were initiated by the addition of purified enzyme to a final concentration of 20 nM.

Microsoft Excel was used to plot and analyze the data to determine kinetic parameters. Initial reaction rates were calculated by least-squares linear regression. Lineweaver–Burke plots suggested initial guesses for the kinetic parameters and the type of inhibition to be fitted. Least-squares non-linear regression used standard models, including the Michaelis–Menten equation and variations thereof describing competitive (1), non-competitive (2), uncompetitive (3) and mixed (4) inhibition to determine kinetic parameters and estimate their errors. Fits to other models, including those for slow- and tight-binding inhibitors (Szedlacsek & Duggleby, 1995), were considered and attempted, but the regressions either did not converge or yielded parameters that reduce the models to simpler expressions.

$$v = \frac{V_\mathrm{max}[S]}{[S] + K_\mathrm{m}^\mathrm{app}\left[1 + \left(\frac{[I]}{K_I^C}\right)\right]} \quad (1)$$

$$v = \frac{V_\mathrm{max}[S]}{([S] + K_\mathrm{m}^\mathrm{app})\left[1 + \left(\frac{[I]}{K_I^N}\right)\right]} \quad (2)$$

$$v = \frac{V_\mathrm{max}[S]}{K_\mathrm{m}^\mathrm{app} + [S]\left[1 + \left(\frac{[I]}{K_I^U}\right)\right]} \quad (3)$$

$$v = \frac{V_\mathrm{max}[S]}{K_\mathrm{m}^\mathrm{app}\left[1 + \left(\frac{[I]}{K_I^C}\right)\right] + [S]\left[1 + \left(\frac{[I]}{K_I^U}\right)\right]} \quad (4)$$

2.4. Crystallography

We predicted that PfDHODH would crystallize under conditions similar to those observed in the crystallization of HsDHODH (Liu *et al.*, 2000). Hits from high ammonium sulfate concentration/low-pH screens were screened with additives and detergents (Hampton) to improve crystallization conditions. Results from one detergent screen suggested C_8E_5 as an additive instead of the amine-β-oxides used for crystallizing HsDHODH. Dynamic light-scattering experiments (data not shown) confirmed that a solution of 1 mM PfDHODH became monodisperse upon addition of C_8E_5.

Table 1
PfDHODH diffraction data statistics.

Values in parentheses are for the highest resolution shell (2.53 > d > 2.40 Å).

Wavelength (Å)	0.9474
Oscillation (φ) (°)	1.0
Exposure (s)	20
Resolution (Å)	50 > d > 2.40
Total/unique reflections	107421/23068
Completeness (%)	98.0 (99.8)
$\langle I/\sigma(I)\rangle$	8.6 (2.3)
Multiplicity	4.7 (4.7)
R_sym (%)	7.4 (32.4)
Unit-cell parameters (hexagonal) (Å, °)	$a = b = 105.4$, $c = 276.6$, $\alpha = \beta = 90$, $\gamma = 120$
Unit-cell parameters (rhombohedral) (Å, °)	$a = b = c = 110.5$, $\alpha = \beta = \gamma = 57.0$

Diffraction-quality crystals of PfDHODH were grown using the sitting-drop vapor-diffusion technique. The substrates dihydroorotate and A77 1726 were solubilized in DMSO (50 mM) and then added to a final concentration of 2 mM each in the concentrated (20 mg ml^{-1}) protein solution. The detergent C_8E_5 was also added to increase its final concentration to 14 mM. As with HsDHODH, no crystallization is observed without the presence of these additives in solution (Liu *et al.*, 2000). The spiked protein solution was then mixed with an equal volume of reservoir solution [41%(w/v) ammonium sulfate and 100 mM sodium acetate pH 4.3–4.4] and equilibrated against 0.5 ml reservoir solution at 277 K.

Crystals were frozen in liquid nitrogen using a cryoprotectant consisting of 30%(v/v) glycerol, 41%(w/v) ammonium sulfate and 100 mM sodium acetate pH 4.3–4.4. Diffraction data were collected at 100 K on the A1 beamline at the Cornell High Energy Synchrotron Source (CHESS) using an ADS Quantum 4 CCD detector. All data were reduced with *DPS* (Rossmann & van Beek, 1999) (Table 1). The hexagonal plates were found to have *R*32 symmetry with one molecule per asymmetric unit, a solvent content of 60.9% and unit-cell parameters $a = b = 105.4$, $c = 276.6$ Å using hexagonal coordinates.

Molecular replacement with *MOLREP* (Collaborative Computational Project, Number 4, 1994) using HsDHODH (PDB code 1d3h, 35% sequence identity in the search region) as a search model provided an initial solution for prime-and-switch phasing with *RESOLVE* (Terwilliger, 2001*a*,*b*). The resulting model required extensive manual rebuilding with *O* (Jones *et al.*, 1991; Kleywegt & Jones, 1996). Electron-density maps ($F_\mathrm{o} - F_\mathrm{c}$) displayed well defined density for the substrates and the prosthetic group before including them in *CNS* (Brünger *et al.*, 1998) refinement (Table 2) using parameters from the Hetero-Compound Information Centre, Uppsala (Kleywegt & Jones, 1998). Molecular graphics were created with *ALSCRIPT* (Barton, 1993), *SPOCK* (Christo-

Table 2
Refinement statistics, $33.5 > d > 24$ Å.

Values in parentheses are for the highest resolution shell ($2.55 > d > 2.40$ Å).

No. of reflections (work/test)	21786 (3649)/1139 (186)
Completeness (%)	97.3 (98.7)
$I/\langle\sigma(I)\rangle/\langle I/\sigma(I)\rangle$	21.8 (7.2)/30.4 (9.0)
Total No. of atoms	3282
No. of protein atoms	2956
No. of ligand atoms	114
No. of water atoms	212
$R/R_{\rm free}$ (%)	20.1 (22.0)/24.3 (27.8)
Luzzati plot/cross-validated	0.24/0.31
SIGMAA/cross-validated	0.19/0.25
R.m.s. bond lengths (Å)/angles (°)	0.007/1.42
R.m.s. dihedral/improper angles (°)	21.2/ 0.77
R.m.s. *B* bonds/angles (Å^2)	
Main chain	1.42/2.35
Side chain	2.24/3.38
Ramachandran plot (%)	
Most favored	91.2
Additionally allowed	7.9
Generously allowed	0.6
Disallowed	0.3

pher, 1998), *POVScript+* (Fenn *et al.*, 2003) and *POV-Ray* (The POV-Ray Team, 2003).

3. Results

3.1. Gene synthesis, expression and purification

Our protocol consistently yielded about 10 mg of PfDHODH per litre of growth medium. THESIT detergent was chosen as an initial extraction detergent because it has no absorbance at 280 nm and is inexpensive for use in the large preparations required for structural studies. As an optional enrichment step, riboflavin can be added to the growth medium.

3.2. Enzyme kinetics

The concentration of CoQ_1 was varied at saturating concentration of dihydroorotate to determine the values of the Michaelis–Menten constant ($K_{\rm m} = 13.1 \pm 1.6\ \mu M$), the catalytic rate ($k_{\rm cat} = 6.15 \pm 0.15\ {\rm s}^{-1}$) and the specificity constant ($k_{\rm cat}/K_{\rm m} = 0.47 \pm 0.06\ {\rm s}^{-1}\ \mu M^{-1}$). The Michaelis–Menten constant is consistent with published values, but the catalytic rate and the specificity constant are about three times greater than expected and the quinone substrate used in our experiments is different from that used previously (Baldwin *et al.*, 2002). These values vary inversely with the concentration of enzyme used in the experiment, so they also reflect the error in the measured protein concentration.

Extensive measurements have been made of the inhibition of HsDHODH by several compounds, including A77 1726 (Bruneau *et al.*, 1998; Davis *et al.*, 1996; Knecht & Löffler, 1998; McLean *et al.*, 2001), brequinar (Bruneau *et al.*, 1998; Chen *et al.*, 1986, 1990, 1992; Cleaveland *et al.*, 1996; Knecht *et al.*, 2000; Knecht & Löffler, 1998, 2000*a*; Lakaschus & Löffler, 1992; McLean *et al.*, 2001; Peters *et al.*, 1987) and atovaquone (Knecht *et al.*, 2000; Knecht & Löffler, 2000*a*; Seymour *et al.*, 1994). Similar measurements have been made for rat DHODH (RrDHODH) with A77 1726 (Kobayashi *et al.*, 2001), brequinar (Knecht *et al.*, 2000; Knecht & Löffler, 1998; Kobayashi *et al.*, 2001) and atovaquone (Knecht *et al.*, 2000; Knecht & Löffler, 2000*a*). Of these, only the inhibitory effect of atovaquone has been measured for PfDHODH (Baldwin *et al.*, 2002; Seymour *et al.*, 1994). Comparison of DHODH inhibition for a given compound demonstrates the effect of differences in the quinone-binding pocket that give rise to specificity. These measurements have been summarized in Table 3 (the structures of the inhibitors are shown in Fig. 3).

Table 3
Inhibition constants demonstrate species-related preferential inhibition.

$K_{\rm i}$, approximate inhibition constant (n*M*); literature references from which these values are derived are given in §3.2 of the text. Structures are shown in Fig. 3.

Compound	Structure	Human	Rat	*P. falciparum*
A77 1726	Fig. 3(*a*)	∼100	∼20	∼10000
Brequinar	Fig. 3(*b*)	∼10	∼30	>1000000
Atovaquone	Fig. 3(*c*)	∼2000	∼75	>500000

Least-squares analyses of inhibition assays for PfDHODH using the novel asymmetric terphenyl compounds atovaquone, brequinar and DPC-AE661100 did not converge for any regression model. The fitting failure is probably a consequence of the low concentration of inhibitor used in the assay compared with the value of its apparent inhibition constant. Because we were only interested in potent inhibitors, we did not repeat the assays at higher inhibitor concentrations. Instead, we employed a crude assay using DCIP buffer. In the presence of an inhibitor, the buffer will remain dark blue, even after 10 min. If the compound being assayed is not functioning as an inhibitor at a given concentration, the buffer will become colorless in less than a minute. The buffer will become dark blue again after about 15 min owing to the reoxidation of DCIP by molecular oxygen.

Some of the novel asymmetric terphenyl compounds displayed modest mixed inhibition of HsDHODH ($\sim 100 > K_{\rm i} > \sim 3\ \mu M$), but none were effective against PfDHODH, even at a concentration of 1 m*M*. Brequinar and DPC-AE661100 are potent inhibitors of HsDHODH ($K_{\rm i} < 10$ n*M*), but had no effect on PfDHODH activity, even at a concentration of 1 m*M*. Although the *in vivo* target of atovaquone is

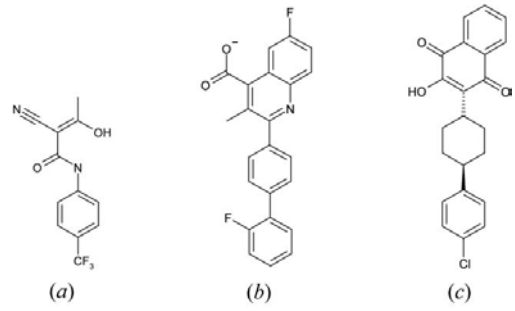

Figure 3
Structures of the inhibitors (*a*) A77 1726, (*b*) brequinar and (*c*) atovaquone.

not DHODH (Fry & Pudney, 1992; Seymour *et al.*, 1994), HsDHODH is inhibited by it *in vitro* ($K_i \simeq 20\ \mu M$). Seymour and coworkers used a complicated *in vitro* assay in which the downstream production of UMP from radiolabeled dihydroorotate is measured over time to report that atovaquone also inhibits PfDHODH ($K_i = 27\ \mu M$). In contrast, using the same DCIP assay that was employed to determine the K_i for HsDHODH, PfDHODH seems to be inhibited by atovaquone only at concentrations greater than 500 μM. The rate data for the inhibition of PfDHODH by A77 1726 could be fitted to both the noncompetitive and mixed models of inhibition. The noncompetitive model yielded an inhibition constant of $11.1 \pm 0.5\ \mu M$. The mixed model indicated a specific or competitive inhibition constant of $7.1 \pm 1.9\ \mu M$ and a catalytic or uncompetitive inhibition constant of $12.7 \pm 1.4\ \mu M$. Errors represent the standard error of the fit. Thus, A77 1726 inhibits PfDHODH about 100 times less potently than HsDHODH ($K_i \simeq 100$ nM).

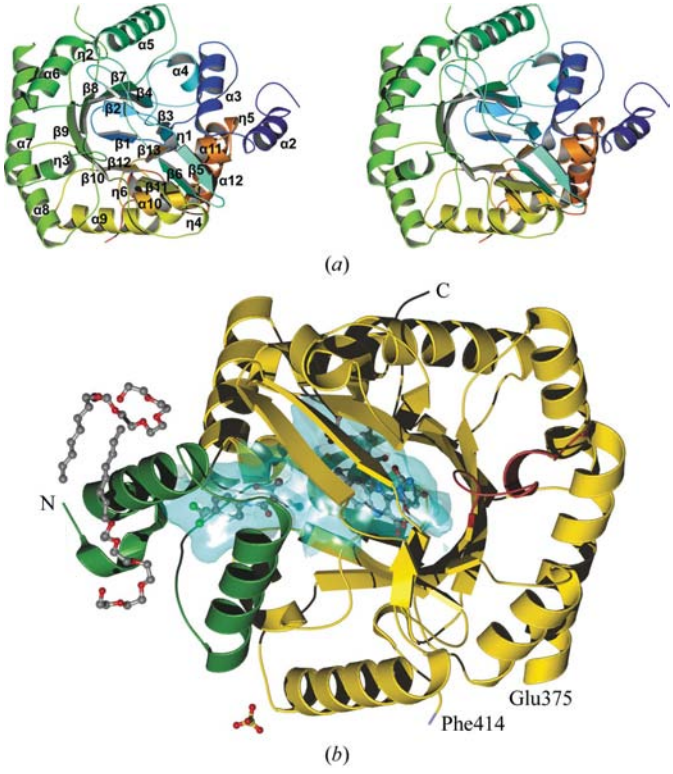

Figure 4
The overall structure of PfDHODH. (*a*) Steroview of PfDHODH. Labels for secondary structure were assigned successively from the N-terminus (blue) to the C-terminus (red). (*b*) Location of small molecules in PfDHODH (structure rotated 180° in the plane compared with *a*). PfDHODH assumes an α/β-barrel fold (gold). The dihydroorotate-binding site (cyan) is inside the barrel. Dihydroorotate stacks against the internal FMN. The quinone-binding site is formed at the interface of the N-terminal helices (green) and the core α/β-barrel. A previously identified flexible loop (red) covers the dihydroorotate-binding site. The flexible loop insert unique to PfDHODH is mostly absent (Glu375–Phe414) from the structure. The inhibitor A77 1726 was cocrystallized with the protein and was found in the quinone-binding site (cyan). Also shown are two detergent molecules and a sulfate ion, which mediate crystal contacts.

3.3. Overall structure

The overall α/β-barrel structure (Fig. 4) of PfDHODH is similar (backbone r.m.s. displacement: human = 1.0 Å, rat = 1.0 Å, *E. coli* = 1.1 Å) to that of other family 2 DHODHs (Hansen *et al.*, 2004; Liu *et al.*, 2000; Nørager *et al.*, 2002). The core of the barrel is formed by eight parallel β-strands which are surrounded by eight α-helices. Short 3_{10}-helices were identified using *DSSP* (Kabsch & Sander, 1983) and *STRIDE* (Frishman & Argos, 1995) at the N- and C-termini and at junctions between some of the β-strands and α-helices. Short antiparallel β-strands cap both ends of the barrel. One of these caps lies flat on the N-terminal ends of the β-barrel, forming a lid. The other cap protrudes from the C-terminal loops of the β-barrel and forms a platform whose intersection with the α/β-barrel core is the site of reaction. The platform supports a flavin mononucleotide (FMN) prosthetic group that segregates the dihydroorotate-binding site to the mouth of the barrel and the quinone-binding tunnel to the outer surface of the barrel. The quinone-binding site is blanketed by the two α-helices of the N-terminal domain. These α-helices are loosely tethered to the core domain by a poorly defined loop of 15 residues. The inhibitor probably stabilizes a limited set of conformations for these α-helices in the crystal lattice because, as with HsDHODH, the presence of inhibitor was required for crystallization.

Long insertions are common in *P. falciparum* proteins and their significance is not clear (Anders, 1986; Aravind *et al.*, 2003). PfDHODH contains a 44-residue insertion (376–419) in the core domain. This insertion does not change the α/β-barrel structure of the core and is at least 30 Å away from the nearest catalytic moiety. Judging by the lack of electron density for most of this insertion (376–413), it does not have a well defined secondary structure. This observation is consistent with those from other *P. falciparum* protein structures that also have these characteristic insertions (Anders, 1986; Aravind *et al.*, 2003). Although there was no interpretable electron density for the insertion, there is a large region between individual protein molecules as they are arranged in the crystal lattice that could accommodate these disordered residues without interfering with crystal packing.

3.4. Small molecules

Strong electron density indicated the presence of a sulfate ion along a threefold rotation axis, where it mediates contacts between the three symmetry-related molecules *via* hydrogen bonds to $Lys_{Pf}193$ and $Tyr_{Pf}194$. Unmistakable, but not completely defined, electron density designated two molecules of C_8E_5 detergent near the same symmetry axis. Both detergent molecules mediate contacts between the N-terminal domains of the other two symmetry-related molecules and may mimic the protein's interaction with the mitochondrial membrane. The polyoxyethylene moiety of one of the detergent molecules assumes a crown ether-like conformation, coordinating $Lys_{Pf}173$ and mediating contacts to a symmetry-related molecule (closest approach $Gly_{Pf}554$). The acyl tail of the coordinating detergent molecule wraps around the first

helix of the quinone-binding domain. The second detergent molecule lies antiparallel to the first, with its hydrophobic tail near that of the first molecule and the polyoxyethylene moiety in a groove between the two helices that form the roof of the quinone-binding tunnel.

Well defined electron density suggested the presence of FMN and orotate in the core of the protein. The presence of the two oxidized species lacks physiological relevance (McLean *et al.*, 2001), but the structure does serve to define the locations of their binding sites. The sites are found in almost exactly the same places as in HsDHODH (FMN r.m.s. = 0.79 Å, orotate r.m.s. = 0.53 Å) and with similar hydrogen-bonding patterns to the conserved residues that make up the sites. The temperature factors for the orotate and FMN are less than 25 $Å^2$, which are among the lowest values in the structure. The structure suggests no clear mechanism for the relaying of electrons from the FMN to the respiratory quinone molecule, although the strictly conserved $Tyr_{Pf}528$ may play a role.

3.5. Quinone-binding tunnel

The inhibitor A77 1726 is bound in the putative quinone-binding tunnel formed by the N-terminal domain (Fig. 5). Our structure-based sequence alignment (Fig. 2) reveals the variability in the residues that make up the quinone-binding tunnel. Some of these nonconserved residues alter the shape and chemical composition of the tunnel, resulting in distinctive structural features at the mouth, waist and end of the quinone-binding tunnel. Other nonconserved residues contribute to the amphipathic character of the domain as a whole, but do not change the shape of the tunnel.

The r.m.s. backbone displacement for the domain when aligned with the structure of HsDHODH bound to A77 1726 (PDB code 1d3h) using the entire backbone is 3.6 Å. When the domain alone is aligned, most of it (170–198) overlaps well (r.m.s. backbone displacement: 1.2 Å). The domain structures diverge at the N-terminus of the first helix (165–170), where the r.m.s. backbone displacement is 4.8 Å, yielding an average r.m.s. backbone displacement of 2.2 Å for the domain. A slight kink in the first helix at $Leu_{Hs}42$ broadens the mouth of the quinone-binding tunnel in HsDHODH and is responsible for the overlap divergence. The first helix is linear in PfDHODH, bringing the N-terminus of this helix closer to the C-terminus of the second helix and sealing off the mouth of the quinone-binding tunnel with the help of the substitution of $Phe_{Pf}171$ for $Leu_{Hs}42$ and $Met_{Pf}536$ for $Pro_{Hs}364$.

A pair of residues in the waist of the quinone-binding tunnel work in concert to skew the alignment of the trifluoromethylphenyl tail of A77 1726 in PfDHODH with respect to its position in HsDHODH. In HsDHODH, $Met_{Hs}43$ on the first helix pushes A77 1726 to occupy a space left available by

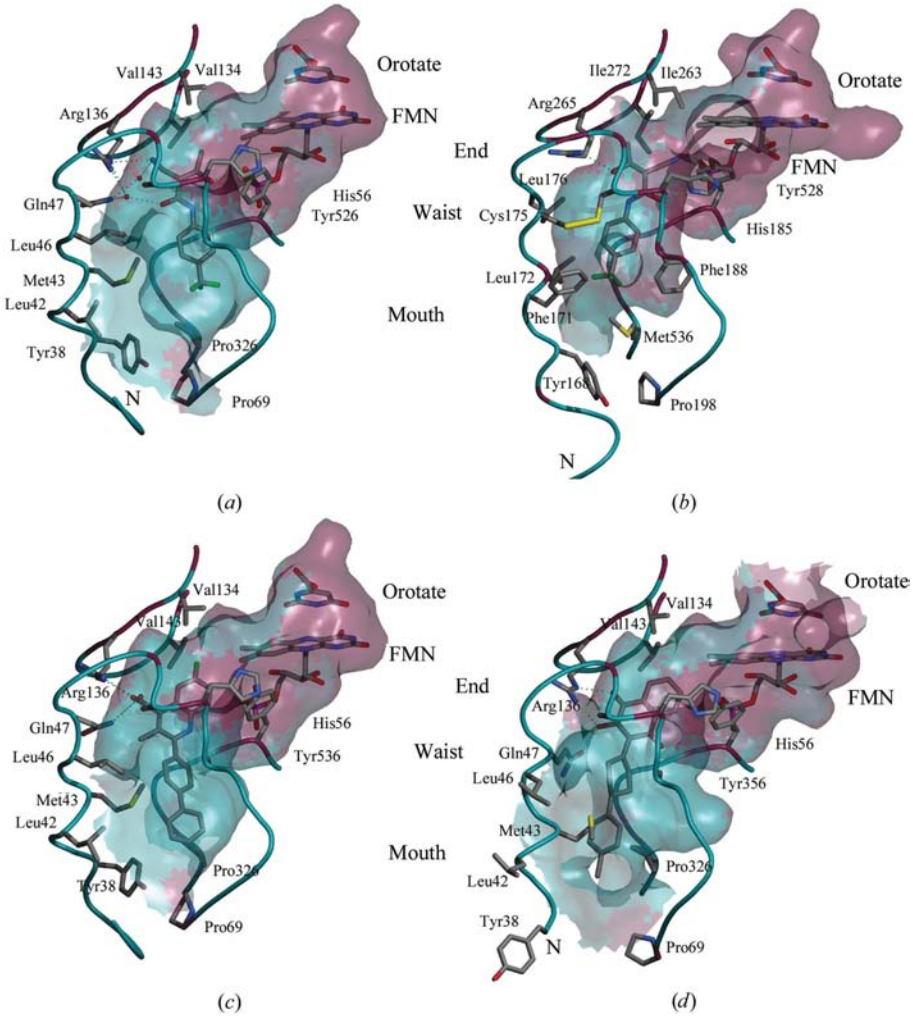

Figure 5
Comparison reveals significant differences between mammalian DHODH and PfDHODH. (*a*) HsDHODH bound to A77 1726, (*b*) PfDHODH bound to A77 1726, (*c*) HsDHODH bound to a brequinar analog, (*d*) RrDHODH bound to atovaquone. The HsDHODH structures show the primary, higher affinity subsite. The PfDHODH and RrDHODH structures illustrate the secondary, lower affinity subsite. Burgundy coloring indicates residues in the C^{α} trace or molecular surface that are identical in PfDHODH and either HsDHODH or RrDHODH. Aqua coloring indicates non-identical residues. The mouth of the quinone-binding tunnel is wide open in HuDHODH and closed owing to non-conserved residues $Phe_{Pf}171$ and $Met_{Pf}536$ in PfDHODH. A phenylalanine residue ($Phe_{Pf}188$) in the waist region prevents A77 1726 from binding to PfDHODH in the same orientation as it binds to HsDHODH. The substitution of a leucine residue ($Leu_{Pf}176$) in the end of the tunnel in PfDHODH removes a potential hydrogen-bonding partner. Larger hydrophobic residues ($Ile_{Pf}263$ and $Ile_{Pf}272$) near the FMN constrict the end of the tunnel. The changes in the quinone-binding pocket led to changes in the binding orientation of A77 1726.

$Ala_{Hs}59$ on the second helix. In PfDHODH, $Met_{Hs}43$ and $Ala_{Hs}59$ are replaced by $Leu_{Pf}172$ and $Phe_{Pf}188$, respectively. The substitution of $Phe_{Pf}188$ for $Ala_{Hs}59$ on the second helix pushes the tail of A77 1726 to occupy a space left open by $Leu_{Pf}172$ on the first helix. This pushing of the tail of A77 1726 ratchets the functional groups at the other end of the inhibitor around with respect to their positions in the human structure, disrupting hydrogen bonding to conserved residues ($His_{Pf}185$, $Arg_{Pf}265$, $Tyr_{Pf}528$) at the end of the tunnel. The substitution of a leucine residue ($Leu_{Pf}176$) in PfDHODH for a glutamine residue ($Gln_{Hs}47$) at the end of the tunnel removes a hydrogen-bonding partner found in HsDHODH. Finally, $Val_{Hs}134$ and $Val_{Hs}143$ are conservatively substituted for $Ile_{Pf}263$ and $Ile_{Pf}272$ at the end of the tunnel in PfDHODH. These larger hydrophobic groups decrease the size of the cavity near the FMN and push A77 1726 slightly back towards the mouth of the tunnel.

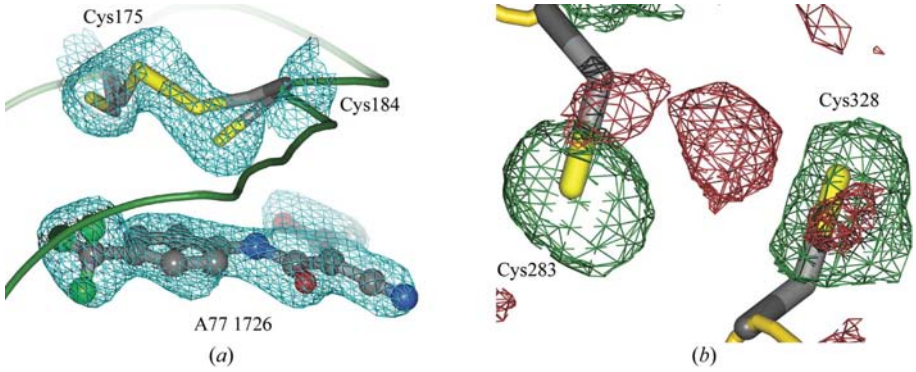

Figure 6
Radiation damage disintegrates disulfide bridges. (*a*) A combination of two reduced cysteines ($Cys_{Pf}175$ and $Cys_{Pf}184$) and a disulfide bridge, each with reduced occupancy, best satisfies the strong electron density (contoured at 1.5σ) found near the quinone-binding site. Electron density is also shown for A77 1726. (*b*) An $F_{obs} - F_{obs}$ difference map was calculated using the first 25 and last 29 frames of the data set to see if the positions of the S atoms changed over the course of data collection owing to radation damage. A distinct change was observed in the disulfide bridge between $Cys_{Pf}283$ and $Cys_{Pf}328$ (contoured at $\pm 2\sigma$).

The differences in shape and chemical environment between the quinone-binding tunnels of PfDHODH and HsDHODH have dramatic consequences for the binding of A77 1726. To better satisfy hydrogen bonding to the conserved residues, the inhibitor binds in a configuration that can most easily be thought of as a 180° rotation about its long axis with respect to its position in HsDHODH. As with HsDHODH, conserved residues $His_{Pf}185$, $Arg_{Pf}265$ and $Tyr_{Pf}528$ participate in hydrogen bonding to the inhibitor at the end of the tunnel; however, hydrogen bonding to HsDHODH involves long-distance water-mediated contacts and no water is found in the PfDHODH binding tunnel, suggesting a closer fit of the inhibitor to the tunnel. The new hydrogen-bonding pattern of ligand binding in PfDHODH appears more favorable than that found in HsDHODH, but the binding of A77 1726 to PfDHODH is two orders of magnitude weaker than to HsDHODH. This disparity suggests that binding is dominated by hydrophobic interactions, whereas hydrogen-bond complementarity provides quinone specificity.

3.6. Disulfide bonds and the oxidation state of the protein

Two disulfide bonds are found in PfDHODH. The first is $Cys_{Pf}283$–$Cys_{Pf}328$ and is located more than 20 Å away from the inhibitor molecule. The other pair of cysteines ($Cys_{Pf}175$–$Cys_{Pf}184$) is unique to *Plasmodium* and provides a disulfide bond in the waist of the quinone-binding tunnel. This bridge locks the turn of the α-helices at the C-terminus of the first helix and the N-terminus of the second helix of the N-terminal domain. The density describing this disulfide bond is among the strongest in the whole structure and therefore must be addressed. The disulfide bond observed in the quinone-binding region might be an artifact of the crystallization conditions, but at least its modeling and time-dependent behavior merit attention. Although a disulfide bond can be formed with an acceptable conformation (Srinivasan *et al.*, 1990), a disulfide alone cannot account for all the strong density in this region. Several alternative models were proposed, including the presence of zinc or another metal ion, but a model that includes both a disulfide bond and two reduced cysteines, each with partial occupancy, best satisfies the electron density (Fig. 6*a*).

Reducing agents were not used in any buffer and crystals were grown, harvested and cryoprotected in an molecular oxygen-containing environment, so it is likely that the disulfide bonds were uniformly present in the crystal before exposure to X-ray radiation. The data were collected over the course of more than 2 h total exposure time on a brilliant synchrotron source. There is some precedent for the ability of large doses of high-energy X-rays to break disulfide bonds (Ravelli & McSweeney, 2000; Sliz *et al.*, 2003). Evidence that this form of radiation damage took place in PfDHODH was suggested by scaling together the first few frames of collected data, scaling together the last few frames of collected data and then calculating an $F_{obs} - F_{obs}$ difference map to see if the positions of the S atoms changed over the course of data collection. A distinct change was observed in the disulfide bond between $Cys_{Pf}283$ and $Cys_{Pf}328$. The bond was apparent at the beginning of the data set, but quickly disintegrated over the course of data collection (Fig. 6*b*). The disintegration of the disulfide bond between $Cys_{Pf}175$ and $Cys_{Pf}184$ is not as obvious, perhaps because the two helices that are held together by the disulfide are stabilized by crystal contacts with other PfDHODH molecules.

Crystallized PfDHODH was found in two isoforms in the same drop: yellow rectangular prisms and colorless hexagonal plates (Fig. 7). The yellow rectangular prisms diffracted poorly, but the colorless hexagonal plates yielded good data.

These two isoforms may reflect the reduced and oxidized states of the flavoprotein. It is not likely that some of protein did not contain FMN because the FMN content of the recombinant enzyme is known to be 0.9 (Baldwin *et al.*, 2002) and because FMN was clearly visible in the electron-density map taken from data collected from the colorless hexagonal plates. It is possible that the colorless plates were so thin that even though they contained oxidized FMN and were yellow in color the coloration was undetectable by eye. Another possible explanation of this observation is that inhibition of the enzymatic activity slowed the oxidation of $FMNH_2$ enough to enable the crystallization process to trap some of the protein in the oxidized state. Despite this possible trapping, the electron density for the flavin clearly suggests the oxidized species. Although colorless at the beginning of the data collection, these hexagonal plates assumed a yellow color by the end of data collection, suggesting that some electron transfer occurred during the course of data collection, perhaps because of radiation damage. It may be that this electron transfer occurred very rapidly at the beginning of the diffraction experiment, resulting in the majority of the data reflecting the oxidized FMN. Because the disulfide bond between $Cys_{Pf}175$ and $Cys_{Pf}184$ is near the FMN- and quinone-binding site, electron transfer from $FMNH_2$ may also be another reason that this disulfide did not disintegrate completely.

4. Discussion

4.1. Malaria

Nearly 50% of the world population is exposed to malaria, with an incidence rate of nearly 400 million that results in over one million deaths annually (Hay *et al.*, 2004). Most of the deaths occur in sub-Saharan Africa among children less than five years of age (Murphy & Breman, 2001; Snow *et al.*, 1999). In the current absence of a vaccine, prophylactic and therapeutic drug use is the only recourse. *P. falciparum* is becoming more resistant to traditional drug treatments, including the novel antimalarial cocktail atovaquone/proguanil (Meprone; Fidock *et al.*, 2004). The antifolate proguanil has been used as an antimalarial agent since 1948. Atovaquone was developed over a period of nearly 40 years as a ubiquinone mimic and potential DHODH inhibitor, but after its introduction in the early 1990s it was discovered that atovaquone acts by disrupting the electron-transport chain through inhibition of cytochrome *b* in Complex III (Fry & Pudney, 1992; Srivastava *et al.*, 1997, 1999). Early reports of atovaquone activity against *de novo* pyrimidine biosynthesis arose from the indirect measurement of inhibition by HPLC of radiolabeled parasites (Hammond *et al.*, 1985). Atovaquone is a reasonably effective treatment for malaria; however, it does not inhibit PfDHODH *in vivo* and thus the enzyme remains a valid antimalarial target that lacks a potent inhibitor.

Figure 7
Different crystal form in the same drop. These two crystals were grown side by side in the same drop. The yellow rectangular prism did not diffract well. The colorless hexagonal crystal diffracted well and provided the data for the structure of PfDHODH.

4.2. Structures explain species-related preferential inhibition

The quinone-binding tunnel in PfDHODH comprises 55 Å^3. The size of the tunnel in human (PDB code 1d3g) and rat (PDB code 1uum) DHODH is much larger (715 and 760 Å^3, respectively). The smaller overall size of the PfDHODH tunnel explains why inhibitors larger than A77 1726, including brequinar, atovaquone, DPC-AE661100 and our series of terphenyl compounds, are ineffective inhibitors of PfDHODH. Specific and distinct structural differences between the three species in the mouth, waist and end of the quinone-binding tunnel are responsible for the species-related preferences for inhibitors that bind in the tunnel (Table 3). Fig. 5 illustrates the shapes of the quinone-binding tunnels and the residues that contribute to preferential inhibition for the three species.

The openness of the mouth is an obvious feature that might contribute to inhibitor preferences. The mouth of the tunnel in PfDHODH is more constricted than in human or rat DHODH. It may be that the smaller size of A77 1726 permits it to more easily pass through the mouth of PfDHODH and bind in its smaller tunnel. In most species, the mouth is probably more open because a major substitution that closes the mouth of PfDHODH ($Met_{Pf}536$) is unique to *Plasmodium* species. Although reasonably flexible, the pushing aside of this methionine by larger inhibitors, such as atovaquone, probably causes them to lose some binding affinity.

The large side chain of $Phe_{Pf}188$ in the waist region of PfDHODH occupies the same position as brequinar in human and rat DHODH, suggesting the major reason for the ineffectiveness of brequinar and our terphenyl compounds on PfDHODH activity. This substitution also contributes to the reduced affinity of PfDHODH for A77 1726.

The end of the quinone-binding tunnel is most conserved between mammalian DHODH and PfDHODH because of the presence of more highly conserved residues. This is as expected because the head group of ubiquinone presumably binds in this region. In each species, the conserved residues ($His_{Pf}185$, $Arg_{Pf}265$, $Tyr_{Pf}528$) occupy about the same position and function as partners in hydrogen bonding to the inhibitor. Additionally, $Gln_{Hs}47$ participates in hydrogen bonding to brequinar, A77 1726, and atovaquone in rat and human

DHODH. In PfDHODH, this residue is a leucine ($Leu_{Pf}176$). The loss of a hydrogen-bonding partner may also be responsible for the lower affinity of PfDHODH for these inhibitors. One strategy for designing a better inhibitor might be to complement the leucine substitution by removing the hydrogen-bonding partner in the inhibitor. However, removal of the 2-hydroxy moiety of atovaquone and other napthoquinones in an attempt to improve binding is unlikely to succeed, because napthoquinones lacking the 2-hydroxy substitution serve as alternate substrates instead of inhibitors of DHODH (Knecht *et al.*, 2000).

The end of the quinone-binding tunnel is slightly smaller in PfDHODH than in mammalian DHODH owing to the increased size of hydrophobic residues ($Ile_{Pf}263$ and $Ile_{Pf}272$) near the FMN. The substitution of isoleucines for valines may be yet another reason for the ineffectiveness of breqinar and the decreased binding of atovaquone in PfDHODH. These residues are probably also the reason for the poor binding of a series of A77 1726 analogues to PfDHODH (Baldwin *et al.*, 2002). Each of these analogues has a large cyclopropyl group that would bump into the hydrophobic wall presented by the isoleucines. This displacement would move the inhibitor beyond the reach of hydrogen-bonding partners and cause the substituted phenyl tail to run into $Phe_{Pf}171$ and $Phe_{Pf}188$, leading to decreased affinity. The finding that a single mutation in *Aspergillus nidulans* DHODH at the position of $Ile_{Pf}263$ confers resistance to agricultural antifungal agent LY214352 strengthens the idea that these residues are important in species-related preferential inhibition (Gustafson *et al.*, 1996).

4.3. Multiple binding modes for inhibition

The mechanism of action of inhibitors of family 2 DHODHs has been thoroughly defined through several kinetics studies, including those already cited and others (Bennett *et al.*, 1979; Cleaveland *et al.*, 1995; Davis *et al.*, 1996; Hudson, 1988; Jaffee *et al.*, 1993; Ullrich *et al.*, 2002; Williamson *et al.*, 1995, 1996). Quantitative structure–activity relationship studies (Batt *et al.*, 1995, 1998, Chen *et al.*, 1990; Knecht & Löffler, 1998; Leban *et al.*, 2004; Pitts *et al.*, 1998; Ren *et al.*, 1998) have also contributed to understanding how these inhibitors bind. These inhibitors engage the same residues and occupy more or less the same position that respiratory quinones presumably do (Hansen *et al.*, 2004). However, kinetic data (McLean *et al.*, 2001; Soliva *et al.*, 2003) and the various structures of DHODH suggest the lack of a unique recognition site. This observation underscores the plasticity of the quinone-binding tunnel and perhaps is related to the indeterminate mixed inhibition kinetics often associated with DHODH inhibitors (Knecht *et al.*, 2000; Knecht & Löffler, 1998, 2000*b*; McLean *et al.*, 2001). Indeed, the different binding modes of inhibitors bound to DHODH demonstrate the adaptability of a few conserved residues in the context of a much larger number of nonconserved residues in the binding tunnel.

The PfDHODH structure demonstrates an example of blocking the activity of the same enzyme from two different species by a significantly altered mode of inhibitor binding. This structure adds support to the hypothesis of multiple binding sites as suggested by kinetic data. Inhibitors bind to DHODH along one of two axes that intersect near the completely conserved $Arg_{Pf}265$. It is possible that these two axes represent two recognition subsites, the first with greater affinity than the second, but both capable of binding DHODH inhibitors. A77 1726 and brequinar analogs bind in the primary subsite of rat and human DHODH. Atovaquone in rat DHODH and A77 1726 in PfDHODH bind in the secondary subsite.

Atovaquone is forced to orient itself along the secondary, lower affinity subsite because of its increased bulk and the chemical character of its hydrophilic Cl atom, which is incompatible with the hydrophobic residues near where it would lie if it bound in the primary subsite. When atovaquone binds in the secondary subsite of RrDHODH, it displaces the first N-terminal helix from the position it takes in all other structures. This displacement occurs from the N-terminus to $Leu_{Rr}46$ by means of a hinge residue ($Gly_{Rr}45$) in the waist region. Atovaquone presumably also binds in the secondary subsite of HsDHODH. However, the displacement of the N-terminal helix is perhaps more difficult in HsDHODH because its hinge residue ($Thr_{Hs}45$) is not allowed as great a range of motion as the hinge in RrDHODH. This difficulty may explain why the inhibition of HsDHODH by atovaquone is more than 25 times weaker than for RrDHODH (Knecht *et al.*, 2000).

The hinge in PfDHODH is a phenylalanine ($Phe_{Pf}174$), compounding the problem. The waist region of PfDHODH contains two cysteine residues that could form a disulfide bond directly adjacent to this phenylalanine. In other species, $Cys_{Pf}175$ is a leucine and $Cys_{Pf}184$ is an alanine. The two cysteines or the leucine and alanine combine to occupy about the same space and volume in every DHODH structure and probably do not impart much specificity to an inhibitor, except when atovaquone pushes the N-terminal helix out and away from the quinone-binding tunnel. If a disulfide bond exists in the native structure of PfDHODH, this bond would be another reason for the ineffectiveness of atovaquone in PfDHODH because the hinge residue would be even more constrained.

Like atovaquone, A77 1726 cannot bind in the primary, higher affinity subsite in PfDHODH. Instead, it is forced to

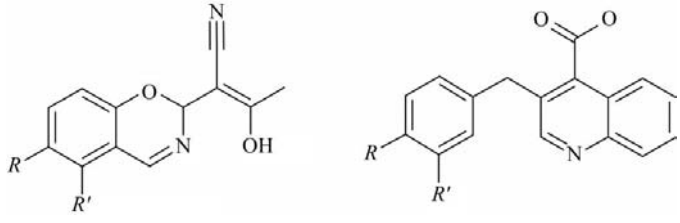

Figure 8
Proposed inhibitors. These proposed inhibitors are based on brequinar and A77 1726, but the phenyl tail is repositioned to avoid collision with $Phe_{Pf}188$. This may permit these compounds to maintain the hydrogen-bonding structure found in the corresponding high-affinity HsDHODH structures.

adopt a second, lower affinity mode of binding owing to the presence of $Phe_{Pf}188$, although other residues certainly contribute, including $Ile_{Pf}263$ and $Ile_{Pf}272$. The result is a 100-fold decrease in binding affinity for A77 1726 between HsDHODH and PfDHODH.

4.4. Finding better inhibitors

This study provides another structure of a family 2 DHODH and analyzes the structural differences between the quinone-binding tunnels of various species. This analysis helps to explain the species-related preferential inhibition observed for various inhibitors of DHODH and provides some constraints for the development of new inhibitors.

Inhibitors for PfDHODH must address the decreased volume at the end of the tunnel and the steric hindrance of $Phe_{Pf}188$. If $Phe_{Pf}188$ were not present, both inhibitors would likely bind PfDHODH with greater affinity, as they do with HsDHODH. Although A77 1726 can change its orientation and bind weakly to PfDHODH, brequinar cannot. A shift in the position of the phenyl tail of A77 1726 and brequinar to avoid $Phe_{Pf}188$ but still bind in their preferred orientation leads to the proposal of two new compounds (Fig. 8). These compounds are based on the hydrogen-bonding moieties of A77 1726 and brequinar, but are less bulky near $Ile_{Pf}263$ and $Ile_{Pf}272$ and avoid $Phe_{Pf}188$. We predict that these changes would permit these compounds to maintain the correct configuration for hydrogen bonding to the conserved trio of $His_{Pf}185$, $Arg_{Pf}265$ and $Tyr_{Pf}528$ and yield greater binding affinity.

Despite these proposed compounds, novel chemotypes will probably be required to develop an effective PfDHODH inhibitor. It is serendipitous that PfDHODH binds A77 1726 at all. Even though some residues that interact with the respiratory quinone are highly conserved, nonconserved residues influence inhibitor binding much more. The two cysteines in the waist region of PfDHODH are unique to *Plasmodium* species. Whether reduced or oxidized in the native protein, these two cysteines are an example of a unique feature of the PfDHODH binding site that could be exploited for inhibitor specificity. Site-directed ligand discovery by 'tethering' (Erlanson *et al.*, 2000; Thanos *et al.*, 2003) libraries of molecular templates to these cysteines may provide one method of probing for new chemotypes specific to PfDHODH.

Despite the abundance of inhibitors that bind in the quinone-binding tunnel, not one has been shown to effectively inhibit PfDHODH. The need for additional tools to combat malaria and the susceptibility of the parasite to DHODH inhibition has encouraged further research into and development of potent and specific PfDHODH inhibitors (Baldwin *et al.*, 2005; Boa *et al.*, 2005). This study provides a structural framework to design a broad screen for new chemotypes. Similar screens are also certainly possible for the potential treatment of many other infectious and autoimmune diseases.

The authors thank NIH CA59021 and the Burroughs Wellcome Fund for their generous support.

References

Anders, R. F. (1986). *Parasite Immunol.* **8**, 529–539.

Aravind, L., Iyer, L. M., Wellems, T. E. & Miller, L. H. (2003). *Cell*, **115**, 771–785.

Baldwin, J., Farajallah, A. M., Malmquist, N. A., Rathod, P. K. & Phillips, M. A. (2002). *J. Biol. Chem.* **277**, 41827–41834.

Baldwin, J., Michnoff, C. H., Malmquist, N. A., White, J., Roth, M. G., Rathod, P. K. & Phillips, M. A. (2005). *J. Biol. Chem.* **280**, 21847–21853.

Barton, G. J. (1993). *Protein Eng.* **6**, 37–40.

Batt, D. G., Copeland, R. A., Dowling, R. L., Gardner, T. L., Jones, E. A., Orwat, M. J., Pinto, D. J., Pitts, W. J., Magolda, R. L. & Jaffee, B. D. (1995). *Bioorg. Med. Chem. Lett.* **5**, 1549–1554.

Batt, D. G., Petraitis, J. J., Sherk, S. R., Copeland, R. A., Dowling, R. L., Taylor, T. L., Jones, E. A., Magolda, R. L. & Jaffee, B. D. (1998). *Bioorg. Med. Chem. Lett.* **8**, 1745–1750.

Bennett, L. L. Jr, Smithers, D., Rose, L. M., Adamson, D. J. & Thomas, H. J. (1979). *Cancer Res.* **39**, 4868–4874.

Björnberg, O., Rowland, P., Larsen, S. & Jensen, K. F. (1997). *Biochemistry*, **36**, 16197–16205.

Boa, A. N., Canavan, S. P., Hirst, P. R., Ramsey, C., Stead, A. M. W. & McConkey, G. A. (2005). *Bioorg. Med. Chem.* **13**, 1945–1967.

Bruneau, J. M., Yea, C. M., Spinella-Jaegle, S., Fudali, C., Woodward, K., Robson, P. A., Sautes, C., Westwood, R., Kuo, E. A., Williamson, R. A. & Ruuth, E. (1998). *Biochem. J.* **336**, 299–303.

Brünger, A. T., Adams, P. D., Clore, G. M., DeLano, W. L., Gros, P., Grosse-Kunstleve, R. W., Jiang, J.-S., Kuszewski, J., Nilges, M., Pannu, N. S., Read, R. J., Rice, L. M., Simonson, T. & Warren, G. L. (1998). *Acta Cryst.* D**54**, 905–921.

Chen, S. F., Papp, L. M., Ardecky, R. J., Rao, G. V., Hesson, D. P., Forbes, M. & Dexter, D. L. (1990). *Biochem. Pharmacol.* **40**, 709–714.

Chen, S. F., Perrella, F. W., Behrens, D. L. & Papp, L. M. (1992). *Cancer Res.* **52**, 3521–3527.

Chen, S. F., Ruben, R. L. & Dexter, D. L. (1986). *Cancer Res.* **46**, 5014–5019.

Christopher, J. A. (1998). *SPOCK: The Structural Properties Observation and Calculation Kit.* http://www.csb.yale.edu/user-guides/graphics/spock/manual/.

Cleaveland, E. S., Monks, A., Vaigro-Wolff, A., Zaharevitz, D. W., Paull, K., Ardalan, K., Cooney, D. A. & Ford, H. Jr (1995). *Biochem. Pharmacol.* **49**, 947–954.

Cleaveland, E. S., Zaharevitz, D. W., Kelley, J. A., Paull, K., Cooney, D. A. & Ford, H. Jr (1996). *Biochem. Biophys. Res. Commun.* **223**, 654–659.

Collaborative Computational Project, Number 4 (1994). *Acta Cryst.* D**50**, 760–763.

Copeland, R. A., Davis, J. P., Dowling, R. L., Lombardo, D., Murphy, K. B. & Patterson, T. A. (1995). *Arch. Biochem. Biophys.* **323**, 79–86.

Copeland, R. A., Marcinkeviciene, J., Haque, T. S., Kopcho, L. M., Jiang, W., Wang, K., Ecret, L. D., Sizemore, C., Amsler, K. A., Foster, L., Tadesse, S., Combs, A. P., Stern, A. M., Trainor, G. L., Slee, A., Rogers, M. J. & Hobbs, F. (2000). *J. Biol. Chem.* **275**, 33373–33378.

Corpet, F. (1988). *Nucleic Acids Res.* **16**, 10881–10890.

Davis, J. P., Cain, G. A., Pitts, W. J., Magolda, R. L. & Copeland, R. A. (1996). *Biochemistry*, **35**, 1270–1273.

Erlanson, D. A., Braisted, A. C., Raphael, D. R., Randal, M., Stroud, R. M., Gordon, E. M. & Wells, J. A. (2000). *Proc. Natl Acad. Sci. USA*, **97**, 9367–9372.

Fenn, T. D., Ringe, D. & Petsko, G. A. (2003). *J. Appl. Cryst.* **36**, 944–947.

Fidock, D. A., Rosenthal, P. J., Croft, S. L., Brun, R. & Nwaka, S. (2004). *Nature Rev. Drug Discov.* **3**, 509–520.
Frishman, D. & Argos, P. (1995). *Proteins*, **23**, 566–579.
Fry, M. & Pudney, M. (1992). *Biochem. Pharmacol.* **43**, 1545–1553.
Gardner, M. J., Hall, N., Fung, E., White, O., Berriman, M., Hyman, R. W., Carlton, J. M., Pain, A., Nelson, K. E., Bowman, S., Paulsen, I. T., James, K., Eisen, J. A., Rutherford, K. & Salzberg (2002). *Nature (London)*, **419**, 498–511.
Gustafson, G., Davis, G., Waldron, C., Smith, A. & Henry, M. (1996). *Curr. Genet.* **30**, 159–165.
Hammond, D. J., Burchell, J. R. & Pudney, M. (1985). *Mol. Biochem. Parasitol.* **14**, 97–109.
Hansen, M., Le Nours, J., Johansson, E., Antal, T., Ullrich, A., Löffler, M. & Larsen, S. (2004). *Protein Sci.* **13**, 1031–1042.
Hay, S. I., Guerra, C. A., Tatem, A. J., Noor, A. M. & Snow, R. W. (2004). *Lancet Infect. Dis.* **4**, 327–336.
Horton, R. M., Hunt, H. D., Ho, S. N., Pullen, J. K. & Pease, L. R. (1989). *Gene*, **77**, 61–68.
Hudson, A. T. (1988). *Antimalarial Hydroxynaphthoquinones, Topics in Medicinal Chemistry*, Vol. 65, edited by P. R. Leeming, pp. 267–283. London: Royal Society of Chemistry.
Jaffee, B. D., Jones, E. A., Loveless, S. E. & Chen, S. F. (1993). *Transplant. Proc.* **25**, *Suppl.* 2, 19–22.
Jensen, K. F. & Björnberg, O. (1998). *Paths Pyrimidines*, **6**, 20–28.
Jones, T. A., Zou, J. Y., Cowan, S. W. & Kjeldgaard, M. (1991). *Acta Cryst.* A**47**, 110–119.
Kabsch, W. & Sander, C. (1983). *Biopolymers*, **22**, 2577–2637.
Kleywegt, G. J. & Jones, T. A. (1996). *Acta Cryst.* D**52**, 829–832.
Kleywegt, G. J. & Jones, T. A. (1998). *Acta Cryst.* D**54**, 1119–1131.
Knecht, W., Henseling, J. & Löffler, M. (2000). *Chem.-Biol. Interact.* **124**, 61–76.
Knecht, W. & Löffler, M. (1998). *Biochem. Pharmacol.* **56**, 1259–1264.
Knecht, W. & Löffler, M. (2000*a*). *Adv. Exp. Med. Biol.* **486**, 267–270.
Knecht, W. & Löffler, M. (2000*b*). *FEBS Lett.* **467**, 27–30.
Kobayashi, K., Nakashima, A., Nagata, H., Nakajima, H., Yamaguchi, K., Sato, S. & Miki, I. (2001). *Inflamm. Res.* **50**, 24–31.
Kovarik, J. M. & Burtin, P. (2003). *Expert Opin. Emerg. Drugs*, **8**, 47–62.
Krogh, A., Larsson, B., von Heijne, G. & Sonnhammer, E. L. L. (2001). *J. Mol. Biol.* **305**, 567–580.
Lakaschus, G. & Löffler, M. (1992). *Biochem. Pharmacol.* **43**, 1025–1030.
Leban, J., Saeb, W., Garcia, G., Baumgartner, R. & Kramer, B. (2004). *Bioorg. Med. Chem. Lett.* **14**, 55–58.
LeBlanc, S. B. & Wilson, C. M. (1993). *Mol. Biochem. Parasitol.* **60**, 349–351.
Liu, S., Neidhardt, E. A., Grossman, T. H., Ocain, T. & Clardy, J. (2000). *Structure Fold. Des.* **8**, 25–33.
Löffler, M., Jockel, J., Schuster, G. & Becker, C. (1997). *Mol. Cell. Biochem.* **174**, 125–129.
Löffler, M., Knecht, W., Rawls, J., Ullrich, A. & Dietz, C. (2002). *Insect Biochem. Mol. Biol.* **32**, 1159–1169.
McLean, J. E., Neidhardt, E. A., Grossman, T. H. & Hedstrom, L. (2001). *Biochemistry*, **40**, 2194–2200.
McRobert, L. & McConkey, G. A. (2002). *Mol. Biochem. Parasitol.* **119**, 273–278.
Marcinkeviciene, J., Rogers, M. J., Kopcho, L., Jiang, W., Wang, K., Murphy, D. J., Lippy, J., Link, S., Chung, T. D., Hobbs, F., Haque, T., Trainor, G. L., Slee, A., Stern, A. M. & Copeland, R. A. (2000). *Biochem. Pharmacol.* **60**, 339–342.
Moller, S., Croning, M. D. R. & Apweiler, R. (2001). *Bioinformatics*, **17**, 646–653.
Murphy, S. C. & Breman, J. G. (2001). *Am. J. Trop. Med. Hyg.* **64**, 57–67.
Nagy, M., Lacroute, F. & Thomas, D. (1992). *Proc. Natl Acad. Sci. USA*, **89**, 8966–8970.
Nørager, S., Jensen, K. F., Björnberg, O. & Larsen, S. (2002). *Structure*, **10**, 1211–1223.
Peters, G. J., Sharma, S. L., Laurensse, E. & Pinedo, H. M. (1987). *Invest. New Drugs.* **5**, 235–244.
Pitts, W. J., Jetter, J. W., Pinto, D. J., Orwat, M. J., Batt, D. G., Sherk, S. R., Petraitis, J. J., Jacobson, I. C., Copeland, R. A., Dowling, R. L., Jaffee, B. D., Gardner, T. L., Jones, E. A. & Magolda, R. L. (1998). *Bioorg. Med. Chem. Lett.* **8**, 307–312.
Ravelli, R. B. & McSweeney, S. M. (2000). *Structure Fold. Des.* **8**, 315–328.
Rawls, J., Knecht, W., Diekert, K., Lill, R. & Löffler, M. (2000). *Eur. J. Biochem.* **267**, 2079–2087.
Ren, S., Wu, S. K. & Lien, E. J. (1998). *Pharm. Res.* **15**, 286–295.
Rossmann, M. G. & van Beek, C. G. (1999). *Acta Cryst.* D**55**, 1631–1653.
Rowland, P., Nielsen, F. S., Jensen, K. F. & Larsen, S. (1997). *Structure*, **5**, 239–252.
Seymour, K. K., Lyons, S. D., Phillips, L., Rieckmann, K. H. & Christopherson, R. I. (1994). *Biochemistry*, **33**, 5268–5274.
Sliz, P., Harrison, S. C. & Rosenbaum, G. (2003). *Structure*, **11**, 13–19.
Snow, R. W., Craig, M., Deichmann, U. & Marsh, K. (1999). *Bull. World Health Organ.* **77**, 624–640.
Soliva, R., Almansa, C., Kalko, S. G., Luque, F. J. & Orozco, M. (2003). *J. Med. Chem.* **46**, 1372–1382.
Sonnhammer, E. L. L., von Heijne, G. & Krogh, A. (1998). *Sixth International Conference on Intelligent Systems for Molecular Biology*, edited by J. Glasgow, T. Littlejohn, F. Major, R. Lathrop, D. Sankoff & C. Sensen, pp. 175–182. Menlo Park, CA: AAAI Press.
Srinivasan, N., Sowdhamini, R., Ramakrishnan, C. & Balaram, P. (1990). *Int. J. Pept. Protein Res.* **36**, 147–155.
Srivastava, I. K., Morrisey, J. M., Darrouzet, E., Daldal, F. & Vaidya, A. B. (1999). *Mol. Microbiol.* **33**, 704–711.
Srivastava, I. K., Rottenberg, H. & Vaidya, A. B. (1997). *J. Biol. Chem.* **272**, 3961–3966.
Sutton, A. E. & Clardy, J. (2001). *Tetrahedron Lett.* **42**, 547–551.
Szedlacsek, S. E. & Duggleby, R. G. (1995). *Methods Enzymol.* **249**, 144–180.
Terwilliger, T. C. (2001*a*). *Acta Cryst.* D**57**, 1755–1762.
Terwilliger, T. C. (2001*b*). *Acta Cryst.* D**57**, 1763–1775.
Thanos, C. D., Randal, M. & Wells, J. A. (2003). *J. Am. Chem. Soc.* **125**, 15280–15281.
The POV-Ray Team (2003). *POV-Ray – the Persistence of Vision Raytracer*, v.3.5x. http://www.povray.org.
Thompson, J. D., Higgins, D. J. & Gibson, T. J. (1994). *Nucleic Acids Res.* **22**, 4673–4680.
Ullrich, A., Knecht, W., Piskur, J. & Löffler, M. (2002). *FEBS Lett.* **529**, 346–350.
Williamson, R. A., Yea, C. M., Robson, P. A., Curnock, A. P., Gadher, S., Hambleton, A. B., Woodward, K., Bruneau, J. M., Hambleton, P., Moss, D., Thomson, T. A., Spinella-Jaegle, S., Morand, P., Courtin, O., Sautes, C., Westwood, R., Hercend, T., Kuo, E. A. & Ruuth, E. (1995). *J. Biol. Chem.* **270**, 22467–22472.
Williamson, R. A., Yea, C. M., Robson, P. A., Curnock, A. P., Gadher, S., Hambleton, A. B., Woodward, K., Bruneau, J. M., Hambleton, P., Spinella-Jaegle, S., Morand, P., Courtin, O., Sautes, C., Westwood, R., Hercend, T., Kuo, E. A. & Ruuth, E. (1996). *Transplant. Proc.* **28**, 3088–3091.